Tabel 2. Material Properties

Materials	Relative Permeability (μ_r)	Bulk Conductivity (S/m)	Mass Density (kg/m^3)
Aluminium	1.000021	3.8×10^7	2689
Iron	4000	1.03×10^7	7870
Copper	0.999991	5.8×10^7	8933
Vacuum	1	0	0

3.0 RESULT AND DISCUSSION

3.1 Verification

Data validation was carried out by re-modelling in accordance with the modeling and simulation of previous research. The validation was carried out by comparing the data to the previous research conducted by Putra (M. R.A. Putra et al., 2019). The goal of this simulation is to determine the braking torque and initial flux. Modeling is done by creating a 3D design using Fusion 360 software. The modeling that will be used for data validation is designed as closely as possible to the design to be compared, so that it can produce an assessment similar to the previous design. Validation will hold the simulation's parameters accountability. Table 3 shows a table of data validation against previous studies.

Table 3. Table of data validation against previous research

Rotating Speed (rpm)	Braking Torque (Nm)		Deviation	
	Putra's Research (M. R.A. Putra et al., 2019)	New Research	(%)	|%|
150	5.086	4.847	4.7	4.7
300	8.300	7.937	4.37	4.37
450	9.429	9.120	3.28	3.28
600	9.383	9.129	2.71	2.71
750	8.828	8.542	3.24	3.24
Average				**3.66**

Table 3 shows that the average deviation in this study is 3.66%. This shows that the results of the comparison of data between previous studies and new studies have a deviation of less than 5%. It can be said that the modeling and simulation results are valid.

3.2 Braking Torque

The simulation results for each variation are shown in Table 4.

Table 4. ECB simulation result data

NO	Rotating Speed (rpm)	Braking Torque (Nm)			
		6 Slots	8 Slots	10 Slots	12 Slots
1	150	8.86	8.99	9.18	9.02
2	300	14.09	14.27	14.51	14.26
3	450	15.52	15.71	15.93	15.72
4	600	14.93	15.12	15.30	15.07
5	750	13.66	13.70	13.80	13.63

It can be seen that the largest braking torque in each variation of the number of slots is found at a rotational speed of 450 rpm and the smallest braking torque in each variation is found at a rotational speed of 150 rpm. The highest braking torque value produced is the number of slots 10 with a speed of 450 rpm of 15.93 Nm. After the speed passes 450 rpm, the resulting data will tend to decrease as the rotational speed increases. This is in accordance with the nature and characteristics of the disc conductor used from non-ferrous material, namely aluminum which causes the emergence of critical speed during the braking process (Kou et al., 2014).

Figure 4 shows the relationship between braking torque and rotational speed. The graph shows that each variation in the number of slots has almost the same graphic pattern. Figure 4 shows that when the number of slots increases from 6 to 8 to 10, the brake torque value increases. However, when 12 slots are added to the conductor plate, the value of brake torque produced in 12 slots is less than the value in 10 slots. The chart tends to show a downward trend after crossing the 450-rpm mark. This occurs as a result of the skin effect (Waloyo et al., 2020). Skin effect is an alternating electric current that appears in the disc conductor so that the current density is formed on the surface of the conductor and will decrease as it gets deeper in the conductor (Taghizadeh Kakhki et al., 2016). With the skin effect on the disc conductor, it will greatly affect the braking torque at high speeds (Waloyo et al., 2020). The addition of a semicircular type conductor disc slot on the ECB braking system has only a small impact on the braking performance of the ECB.

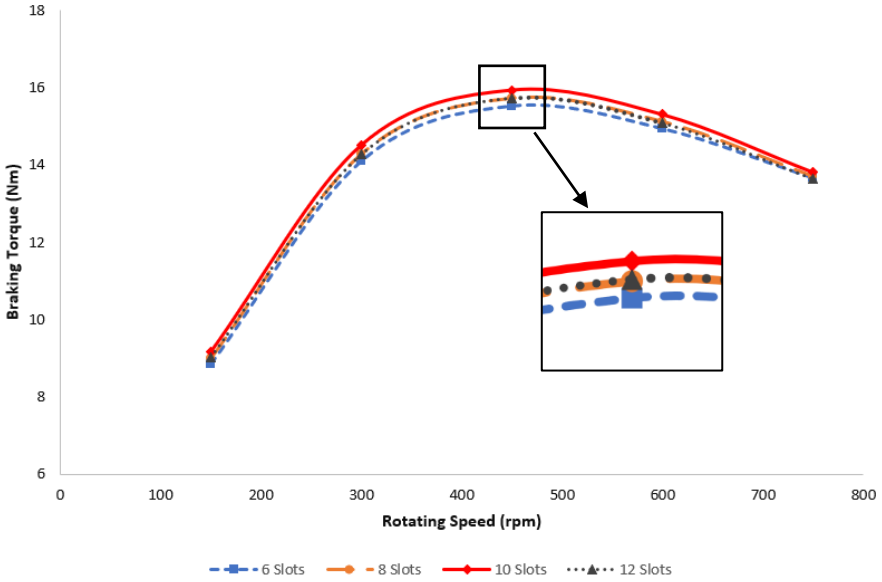

Figure 4. Graph of the relationship between braking torque and rotational speed for each variation

Calculation of braking is done by braking force when the vehicle slows down from a certain speed. The calculation is only to prove the characteristics of the modeling process used, namely regarding the effect of adding a conductor disk slot. At the next stage the braking process can be analyzed with several additional parameters such as rolling resistance, etc.

3.3 Comparation of Magnetic Flux on Variation of Slots

The spread of magnetic flux in each slot variation is shown in Figure 5 below.

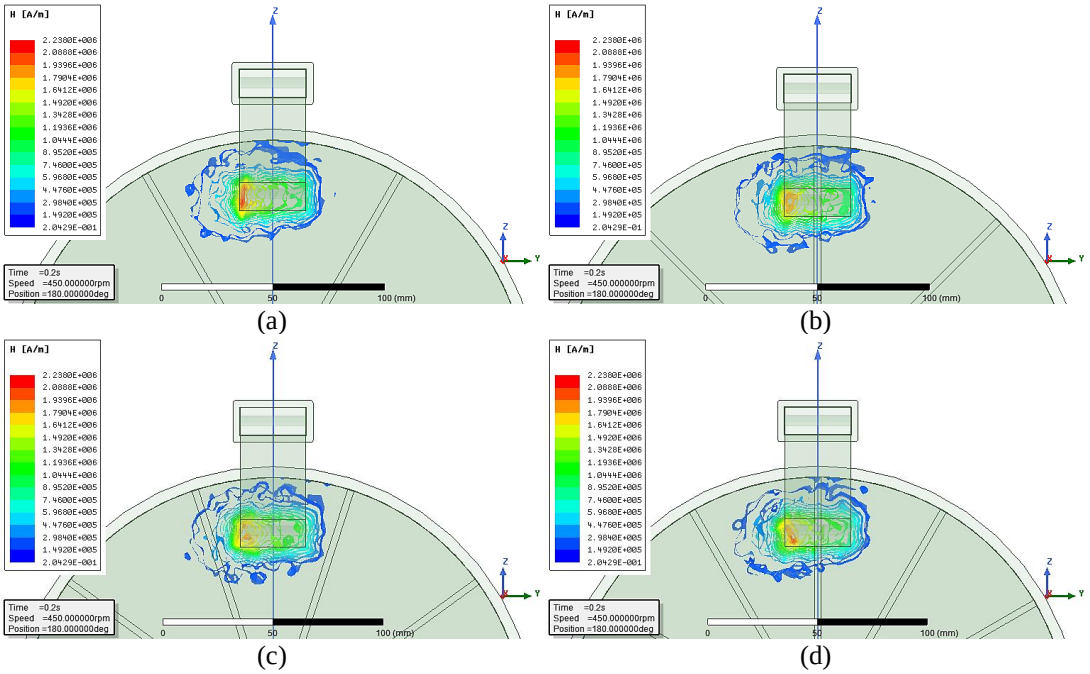

Figure 5. Distribution of magnetic flux in variations of (a) 6 slots, (b) 8 slots, (c) 10 Slots, and (d) 12 slots.

The magnetic flux distribution in Figure 5 in each variation has a magnetic flux distribution that is almost the same or uniform. This makes the addition of the number of half-circle type slots have a less significant effect. The value of the torque produced will also have almost the same value. In addition, the distribution of the magnetic flux is all concentrated in the conductors and cores of the ECB. This phenomenon can be seen in the image in red which indicates that the magnetic field strength is highest in the area closer to the core that carries the electric current.

3.4 Comparation of Magnetic Flux on Rotating Speed

The spread of magnetic flux at each rotational speed variation is shown in Figure 6 below.

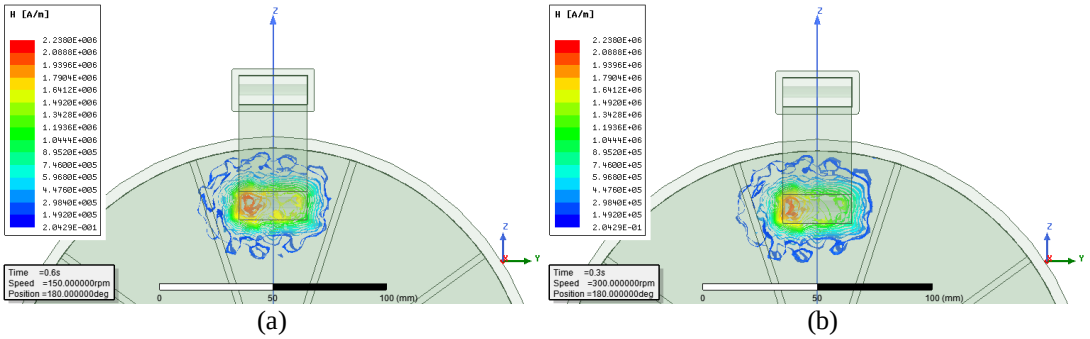

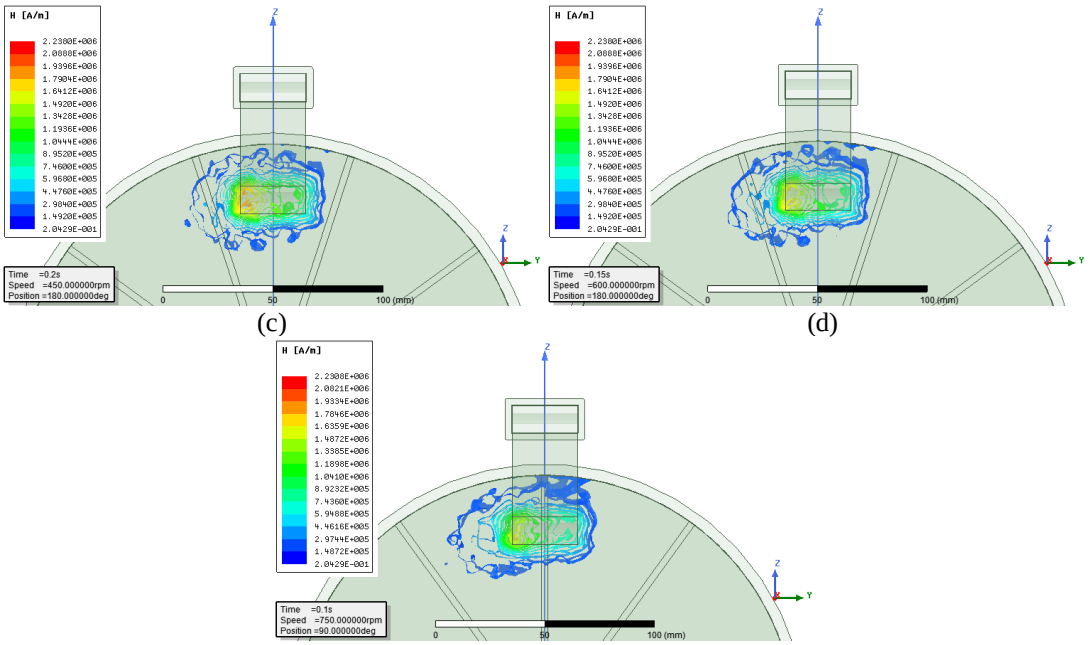

(c) (d)

(e)

Figure 6. Spread of magnetic flux at variations in rotational speed (a) 150 rpm, (b) 300 rpm, (c) 450 rpm, (d) 600 rpm, and (e) 750 rpm.

In Figure 6 it can be seen that the higher the rotational speed, the greater the spread of the magnetic flux on the disc conductor. In addition, the magnetic field at low speeds is more concentrated to the magnetic source (core) and will spread as the speed increases. The magnetic field strength (red color) will disappear with increasing speed. The phenomenon that occurs is related to the skin effect. The skin effect has a significant impact on braking torque and disc rotation speed (Waloyo et al., 2020). Skin effects appear at high rotational speeds which will cause a decrease in the value of the resulting torque. At low speeds, it is seen that the spread of magnetic flux is still around the center of the magnetic field, while at high speeds the distribution of the magnetic field will be further away from the center of the magnetic field and the resulting area will be larger.

4.0 CONCLUSION

From the research that has been done, it can be concluded that the addition of the number of half-circle type slots with slot variations of 6, 8, 10, and 12 slots does not have a significant effect on the torque generated from the simulation. The trend of the graph of adding slots to the conductor has almost the same trend. The highest braking torque value is produced by a variation of 10 slots with a torque value of 15.93 at a speed of 450 rpm. The spread of magnetic flux in the variation of the number of slots has almost the same area shape. It is concluded that the distribution of magnetic flux with variations in the number of slots does not have much effect on ECB braking. In variations in rotational speed, the spread of magnetic flux from low to high-speed changes the shape of the area. The higher the rotational speed, the wider the magnetic flux distribution because the magnetic field strength will spread and be influenced by the skin effect that appears at high speeds.

5.0 ACKNOWLEDGMENT

Thanks to UNS for providing funding and laboratory facilities for ECB research. Thank you to ICE-SEAM 2021 for accepting and presenting the results of this research work.

6.0 REFERENCES

Cho, S., Liu, H. C., Ahn, H., Lee, J., & Lee, H. W. (2017). Eddy Current Brake with a Two-Layer Structure: Calculation and Characterization of Braking Performance. *IEEE Transactions on Magnetics*, *53*(11). https://doi.org/10.1109/TMAG.2017.2707555

Cho, S., Liu, H. C., Lee, J., Lee, C. M., Go, S. C., Ham, S. H., Woo, J. H., & Lee, H. W. (2017). Design and analysis of the eddy current brake with the winding change. *Journal of Magnetics*, *22*(1), 23–28. https://doi.org/10.4283/JMAG.2017.22.1.023

Gerdes, J. C., & Hedrick, J. K. (1999). Brake system modeling for simulation and control. *Journal of Dynamic Systems, Measurement and Control, Transactions of the ASME*, *121*(3), 296–503. https://doi.org/10.1115/1.2802501

Günay, M., Korkmaz, M. E., & Özmen, R. (2020). An investigation on braking systems used in railway vehicles. *Engineering Science and Technology, an International Journal*, *23*(2), 421–431. https://doi.org/10.1016/j.jestch.2020.01.009

Karakoc, K., Suleman, A., & Park, E. J. (2016). Analytical modeling of eddy current brakes with the application of time varying magnetic fields. *Applied Mathematical Modelling*, *40*(2), 1168–1179. https://doi.org/10.1016/j.apm.2015.07.006

Kou, B., Jin, Y., Zhang, H., Zhang, L., & Zhang, H. (2014). Modeling and analysis of force characteristics for hybrid excitation linear eddy current brake. *IEEE Transactions on Magnetics*, *50*(11). https://doi.org/10.1109/TMAG.2014.2323334

Lequesne, B. (1997). Eddy-current machines with permanent magnets and solid rotors. *IEEE Transactions on Industry Applications*, *33*(5), 1289–1294. https://doi.org/10.1109/28.633808

Prayoga, A. R., Ubaidillah, Nizam, M., & Waloyo, H. T. (2019). The Influence of Aluminum Conductor Shape Modification on Eddy-Current Brake Using Finite Element Method. *ICEVT 2019 - Proceeding: 6th International Conference on Electric Vehicular Technology 2019*, 146–150. https://doi.org/10.1109/ICEVT48285.2019.8994005

Putra, M. R.A., Nizam, M., Tjahjana, D. D. D. P., & Waloyo, H. T. (2019). The Effect of Air Gap on Braking Performance of Eddy Current Brakes on Electric Vehicle Braking System. *ICEVT 2019 - Proceeding: 6th International Conference on Electric Vehicular Technology 2019*, 355–358. https://doi.org/10.1109/ICEVT48285.2019.8993987

Putra, Mufti Reza Aulia, Nizam, M., Tjahjana, D. D. D. P., Aziz, M., & Prabowo, A. R. (2020). Application of multiple unipolar axial eddy current brakes for lightweight electric vehicle braking. *Applied Sciences (Switzerland)*, *10*(13). https://doi.org/10.3390/app10134659

Razavi, H. K., & Lampérth, M. U. (2006). Eddy-current coupling with slotted conductor disk. *IEEE Transactions on Magnetics*, *42*(3), 405–410. https://doi.org/10.1109/TMAG.2005.862762

Robert, R. S. (2017). 2D model of axial-flux eddy current brakes with slotted conductive disk rotor. *2017 International Siberian Conference on Control and Communications, SIBCON 2017 - Proceedings*, 0–5. https://doi.org/10.1109/SIBCON.2017.7998501

Rodrigues, O., Taskar, O., Sawardekar, S., Clemente, H., & Dalvi, G. (2016). Design & Fabrication of Eddy Current Braking System. *International Research Journal of Engineering and Technology*, *03*(04), 809–815.

Satya, P. S., Chandra, P. G. S., & Raghavendra, M. B. (2021). A Study about Eddy Current Brakes. *IJTIIR*, 50–55.

Sinmaz, A., Gulbahce, M. O., & Kocabas, D. A. (2016). Design and finite element analysis of a radial-flux salient-pole eddy current brake. *ELECO 2015 - 9th International Conference on Electrical and Electronics Engineering*, *1*, 590–594. https://doi.org/10.1109/ELECO.2015.7394612

Taghizadeh Kakhki, M., Cros, J., & Viarouge, P. (2016). New Approach for Accurate Prediction of Eddy Current Losses in Laminated Material in the Presence of Skin Effect with 2-D FEA. *IEEE Transactions on Magnetics*, *52*(3). https://doi.org/10.1109/TMAG.2015.2481924

Ubaidillah, U., Suwolo, S., Prayoga, A. R., Nizam, M., & Waloyo, H. T. (2020). Magnetic flux distribution and braking torque of a grooved eddy current brake. *2020 2nd International Conference on Computer and Information Sciences, ICCIS 2020*. https://doi.org/10.1109/ICCIS49240.2020.9257655

Waloyo, H. T., Ubaidillah, U., Tjahjana, D. D. D. P., Nizam, M., & Aziz, M. (2020). A novel approach on the unipolar axial type eddy current brake model considering the skin effect. *Energies*, *13*(7), 1–15. https://doi.org/10.3390/en13071561